Journal of Sound and Vibration (2002) **250**(3), 415–430
doi:10.1006/jsvi.2001.3921, available online at http://www.idealibrary.com on IDEAL®

THE APPLICATION OF BALL-TYPE BALANCERS FOR RADIAL VIBRATION REDUCTION OF HIGH-SPEED OPTIC DISK DRIVES

W.-Y. Huang and C.-P. Chao

Department of Mechanical Engineering, Chung-Yuan Christian University, Chung-Li, Taiwan 320. *E-mail: pchao@cycu.edu.tw*

AND

J.-R. Kang and C.-K. Sung

Department of Power Mechanical Engineering, National Tsing Hua University, Hsinchu, Taiwan 300. *E-mail: cksung@pme.nthu.edu.tw*

(*Received* 16 *November* 2000, *and in final form* 11 *May* 2001)

This study is dedicated to the design of a ball-type balancer system installed on the high-speed disk drive in order to reduce radial vibrations of rotors caused by eccentricities of disk's center of gravity and circular runway of the ball balancer. The ball balancer is a promising candidate due to its low cost and capability to completely eliminate radial vibrations under the conditions that runway eccentricity, damping and friction are not present. A mathematical model was established first for the analysis of the dynamics of a rotor–balancer system. The influence of concerned parameters, e.g., runway eccentricity and rolling resistance, on residual vibrations was then explored through solving the equations for steady state solutions. The results were used to evaluate the performance of balancers in terms of vibration reduction. The design guidelines for minimizing the vibrations by controlling the aforementioned concerned parameters were provided based on the parametric analysis conducted. Finally, experimental study was orchestrated and performed to verify the validity of the mathematical model and demonstrate balancer capability for reduction of radial vibrations.

1. INTRODUCTION

Due to unavoidable manufacture tolerance, each disk possesses a small amount of unbalance, which may lead to detrimental dynamic effects under high-speed rotations. The preliminary treatment for reducing radial vibrations of a rotor–disk system consists in balancing the disk while manufacturing. However, as mass production of disks makes the balancing for each disk impossible, auto-balancing devices and active suspensions are the legitimate candidates for reducing vibrations. Compared with the traditional single- or double-level suspensions which are composed of damping washers for isolating vibrations, the auto-balancers directly counteract the unbalanced vibration source by means of the centrifugal forces generated in motion, in which way the balancer system is proven more effective in reducing radial vibrations. Thearel [1, 2] initialized a series of analyses on various types of auto-balancers, wherein the following conclusions were drawn: (1) Lablanc balancer, a fluid-type balancer, fails to achieve a complete vibration elimination, exhibiting

0022-460X/02/080415 + 16 $35.00/0

moderate levels of residual vibrations due to damping; (2) ring balancers have difficulty in regulating the friction between the ring and the shaft; (3) pendulum balancers do not show a satisfactory vibration reduction and have high cost of physical arrangement; (4) ball balancers show excellent balancing effects above the critical speed despite a poor performance below the critical speed.

Among all the aforementioned devices, the ball balancer is superior to the others owing to low friction, low cost and ease to implement. A few studies following Thearel were conducted to further explore the capability of ball balancers. Inoue *et al.* [3] utilized numerical methods to analyze the dynamics of a rotor/balancer system assuming a constant speed. Bövik and Högfors [4] showed that the auto-balancers were applicable to planar and non-planar vibrating rotors. Jinnouchi *et al.* [5] concluded that ball balancers provide excellent balancing above the critical speed, but lead to moderate vibrations at low speeds. This moderate vibration is then enlarged in the neighborhood of the critical speed due to self-excitation. Without constructing equations of motion, Majewski [6] found the negative effects of ball rolling resistance and runway eccentricity on the rotor/balancer system at steady state. Rajalingham and Rakheja [7] first consider contact friction of balancing balls in the model for analysis. Chung and Ro [8] used a variational method to derive equations of motion in polar coordinates. Based on the concepts of ball balancers, several implementation designs were proposed and documented in patents [9–12].

Although several works have been conducted for ball balancers, there is still no complete parametric analysis via the construction of equations of motion which simultaneously accommodates the dynamic effects of runway eccentricity, rolling resistance and drag force on residual vibrations. To achieve the complete parametric analysis, this study starts with the establishment of a mathematical model for describing the dynamics of the rotor/balancer behavior. The steady state solutions were solved for the evaluation of residual vibrations. Then a parametric study is conducted based on the various steady state solutions for different realistic parameter ranges. The effects of three major parameters, runway eccentricity, rolling resistance and drag force, were studied to develop the design guidelines for achieving the smallest level of radial vibration possible. Finally, an experimental set-up was designed and built to verify the validity of the analytical model.

This paper is organized as follows. In section 2, the mathematical model of the rotor/balancer system is established and the dynamic equations governing the lateral motions of the stator and the rotary motions of the balls are formulated. In section 3, a parametric analysis is performed to provide design guidelines. The experimental apparatus and process are described in section 4. The results are compared with theoretical counterparts for validating the correctness of the mathematical model.

2. MATHEMATICAL MODEL

To capture the dynamics of the unbalanced motions, the system that consists of the main components of an optic disk drive can be classified into two categories: rotating and non-rotating parts. The assembly of all rotating parts is called “the equivalent rotor”, containing the disk, magnetic holding device and the rotor of the spindle motor. The assembly of all non-rotating parts is called “the equivalent stator”, containing the foundation structure of the motor, the stator of the spindle motor, the optical pickup head, and its electrical driving unit. Without loss of generality, the following assumptions were made from the outset to facilitate the derivation of a mathematical model.

1. The rotor shaft is treated as a rigid body, leading to no transverse vibrations while in rotation.

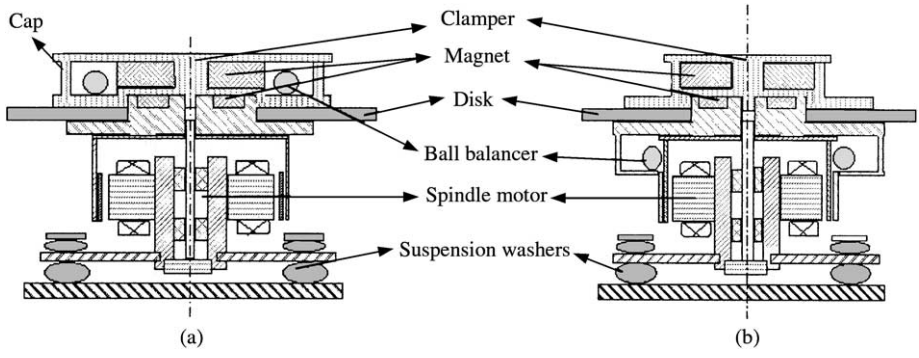

Figure 1. (a) The balls are contained in a cap that is placed on the top of the disk. (b) The balls are integrated into the spindle motor and located under the turntable.

2. The equivalent rotor is treated as a rigid body, i.e., the disk and its magnetic holding device are fixed to each other, exhibiting no relative motion while in high-speed rotations.
3. After the optical pickup unit completes a single tracking process, the stator of the spindle motor, its foundation, the optical pickup head and its electrical driving unit are considered together as a rigid body, i.e., the equivalent stator is treated as a rigid body.

Based on the above assumptions, the motion of the unbalanced rotor is mainly in radial directions due to the horizontal flexibility of the damping washers that constitute the suspension system. The flexibility of these washers is assumed to be well characterized by equivalent linear springs and dampers, denoted by (K_X, K_Y) and (C_X, C_Y) respectively. Note that since the suspension constituted by washers is much more flexible than that of spindle bearing, bearing dynamics is not considered herein. With the assumptions made for the stator–rotor foundation system, ball balancers are then added for radial vibration reduction. Figure 1 shows two generic designs for physical arrangements of balancers [12]. To incorporate the dynamics of balls into the system, the following assumptions are made.

1. The runway shapes as a perfect circle and the balls are assumed to be perfect spheres. While the balls, considered as point masses, move along the runway, they always keep point contacts with outer flanges of the runway, which is true in real operation of steady state due to the centrifugal field.
2. Because of manufacturing tolerance, the center of the circular runway deviates from the rotating center of the rotor by a small distance.
3. The gravitational effect on the balls is small compared to the centrifugal field.
4. No slip occurs while the ball moves since slip friction is much greater than rotational friction.

With the assumptions made for the rotor and the ball balancer, the physical system can be simplified as shown schematically in Figure 2, where, without loss of generality, only one ball with mass m and radius r is considered. To perform the ensuing analysis, the following notations and co-ordinates are defined. G_R and G_S denote the C.G.s of the equivalent rotor and stator respectively. M_R and M_S are the corresponding masses. O_B denotes the C.G. of the ball. O_S is the rotation center of the rotor, i.e., $O_S X_S Y_S$ is fixed to the stator where the

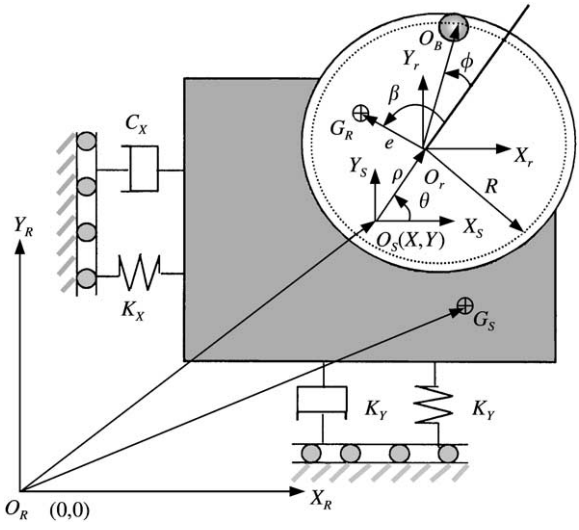

Figure 2. The mathematical model of the rotor.

subscript S denotes the stator. O_R denotes the origin of the inertial co-ordinate $O_R X_R Y_R$, which coincides with O_S while the disk is at rest. Let X and Y be the displacements of O_S defined in $O_R X_R Y_R$ parallel to axes $O_R X_R$ and $O_R Y_R$ respectively. Then, $A = \sqrt{X^2 + Y^2}$ represents the magnitude of the residual radial vibration of the disk-drive assembly. O_r denotes the center of balancer's circular runway and also the origin of the moving co-ordinate $O_r X_r Y_r$. The deviation of O_r from O_S is due to runway eccentricity, which is quantified by ρ. e captures the C.G. eccentricity of equivalent rotor relative to O_r, i.e., $e = |\overline{O_r G_R}|$. θ, defined in co-ordinate $O_S X_S Y_S$, denotes the rotating angle of the disk, i.e., the angle between $O_S X_S$ and $O_S O_r$. β, defined in co-ordinate $O_r X_r Y_r$, denotes the lead angle of the rotor's C.G. location with respect to the current angular position of the rotor. ϕ, defined in co-ordinate $O_r X_r Y_r$, denotes the lead angle of the ball position with respect to the current angular position of the rotor. With sufficiently defined notations, the equations of motion for the ball and rotor system are derived consecutively in the following.

Assuming that no slip occurs between the ball and runway flange, the slip friction force, denoted by F, induces a rolling moment on the ball. Acting on the ball is drag force D due to aerodynamic resistance and rolling resistant moment M_f mainly due to the rolling friction with runway outer flange. Figure 3(a) illustrates the spatial actions of the aforementioned forces. Two accelerations, defined in the inertia co-ordinates $O_R X_R Y_R$, are next derived to capture the dynamics of the ball. As illustrated in Figure 3(b), the net ball acceleration can be decomposed into tangential acceleration a_t and runway flange acceleration a_w. Through the transformations bridging the inertial co-ordinates $O_R X_R Y_R$ and the translating co-ordinates $O_S X_S Y_S$ and $O_r X_r Y_r$, a_t and a_w can be formulated by

$$a_t = R(\ddot{\phi} + \ddot{\theta}) - (\ddot{X} - \rho\ddot{\theta}\sin\theta - \rho\dot{\theta}^2\cos\theta)\sin(\phi + \theta) + (\ddot{Y} + \rho\ddot{\theta}\cos\theta - \rho\dot{\theta}^2\sin\theta)\cos(\phi + \theta), \quad (1)$$

$$a_W = (R + r)\ddot{\theta} - (\ddot{X} - \rho\ddot{\theta}\sin\theta - \rho\dot{\theta}^2\cos\theta)\sin(\phi + \theta) + (\ddot{Y} + \rho\ddot{\theta}\cos\theta - \rho\dot{\theta}^2\sin\theta)\cos(\phi + \theta). \quad (2)$$

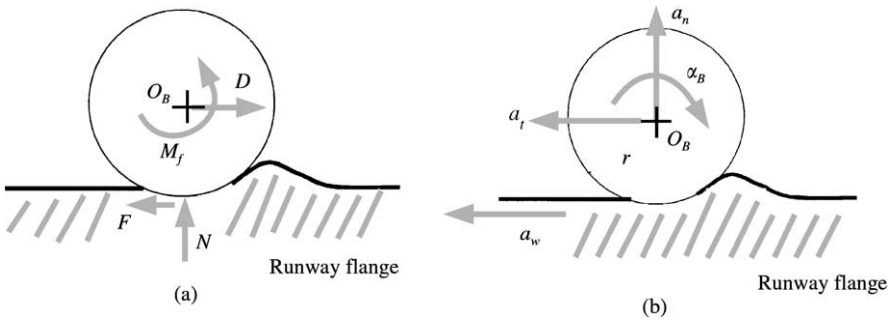

Figure 3. (a) Force equilibrium of a ball. (b) Definitions of ball accelerations.

Balancing the forces and moments acting on the ball as shown in Figure 3(a) leads to two equilibrium equations

$$F - D\,\mathrm{sign}(\dot{\phi}) = ma_t, \tag{3}$$

$$Fr - M_f[-\mathrm{sign}(\dot{\phi})] = I\,\alpha_B, \tag{4}$$

where α_B is the ball angular acceleration relative to runway outer flange. Combining equations (3) and (4) for eliminating F and incorporating equations (1) and (2) into the definition of α_B, $r\alpha_B = a_W - a_i$, the equation of motion for a single ball balancer can be derived as

$$\begin{aligned}\left(m + \frac{1}{r^2}\right) R(\ddot{\phi} + \ddot{\theta}) = m[&(\ddot{X} - \rho\ddot{\theta}\sin\theta - \rho\dot{\theta}^2\cos\theta)\sin(\phi + \theta) \\ &- (\ddot{Y} + \rho\ddot{\theta}\cos\theta - \rho\dot{\theta}^2\sin\theta)\cos(\phi + \theta)] \\ &- D\,\mathrm{sign}(\dot{\phi}) - \frac{M_f}{r}\,\mathrm{sign}(\dot{\phi}) + \frac{(R + r)}{r^2} I\ddot{\theta}.\end{aligned} \tag{5}$$

The expressions of a_t and a_w in equations (1) and (2) enable the derivations of the inertial forces generated by ball motion. These inertial forces are the interactive forces of the ball with the rotor system through the contact with runways, which can be treated as external forces for the rotor system. Then the equations of motion of the equivalent stator for a single ball can be derived easily by balancing the total forces, which are listed as below.

$$\begin{aligned}M\ddot{X} + C_x\dot{X} + K_X X &= M_R[\rho\ddot{\theta}\sin\theta + \rho\dot{\theta}^2\cos\theta + e\ddot{\theta}\sin(\theta + \beta) + e\dot{\theta}^2\cos(\theta + \beta)] \\ &+ m[\rho\ddot{\theta}\sin\theta + \rho\dot{\theta}^2\cos\theta + R(\ddot{\theta} + \ddot{\phi})\sin(\theta + \phi) + R(\dot{\theta} + \dot{\phi})^2\cos(\theta + \phi)],\end{aligned} \tag{6}$$

$$\begin{aligned}M\ddot{Y} + C_y\dot{Y} + K_Y Y &= M_R[-\rho\ddot{\theta}\cos\theta + \rho\dot{\theta}^2\sin\theta - e\ddot{\theta}\cos(\theta + \beta) + e\dot{\theta}^2\sin(\theta + \beta)] \\ &m[-\rho\ddot{\theta}\cos\theta + \rho\dot{\theta}^2\sin\theta - R(\ddot{\theta} + \ddot{\phi})\cos(\theta + \phi) + R(\dot{\theta} + \dot{\phi})^2\sin(\theta + \phi)],\end{aligned}$$

where $M = M_R + M_S + m$. Generalizing the system equations (5) and (6) to consider a rotor system with multiple balls yields

$$\begin{aligned}M\ddot{X} + C_x\dot{X} + K_X X &= M_R[\rho\ddot{\theta}\sin\theta + \rho\dot{\theta}^2\cos\theta + e\ddot{\theta}\sin(\theta + \beta) + e\dot{\theta}^2\cos(\theta + \beta)] \\ &+ m\sum_{i=1}^{n}[\rho\ddot{\theta}\sin\theta + \rho\dot{\theta}^2\cos\theta + R(\ddot{\theta} + \ddot{\phi}_i)\sin(\theta + \phi_i) + R(\dot{\theta} \to \dot{\phi}_i)^2\cos(\theta + \phi_i)],\end{aligned}$$

$$M\ddot{Y} + C_y\dot{Y} + K_Y Y = M_R[-\rho\ddot{\theta}\cos\theta + \rho\dot{\theta}^2\sin\theta - e\ddot{\theta}\cos(\theta+\beta) + e\dot{\theta}^2\sin(\theta+\beta)] \tag{7}$$

$$+ m\sum_{i=1}^{n}[-\rho\ddot{\theta}\cos\theta + \rho\dot{\theta}^2\sin\theta - R(\ddot{\theta}+\ddot{\phi}_i)\cos(\theta+\phi_i) + R(\dot{\theta}+\dot{\phi}_i)^2\sin(\theta+\phi_i)],$$

$$\left(m + \frac{I}{r^2}\right)R(\ddot{\phi}_i + \ddot{\theta}) = m[(\ddot{X} - \rho\ddot{\theta}\sin\theta - \rho\dot{\theta}^2\cos\theta)\sin(\phi_i+\theta) - (\ddot{Y} + \rho\ddot{\theta}\cos\theta - \rho\dot{\theta}^2\sin\theta)$$

$$\cos(\phi_i+\theta)] - D\,\mathrm{sign}(\dot{\phi}_i) - \frac{M_f}{r}\mathrm{sign}(\dot{\phi}_i) + \frac{(R+r)}{r^2}I\ddot{\theta}.$$

3. PARAMETRIC ANALYSIS

3.1. EFFECTS OF RUNWAY ECCENTRICITY

In order to understand the effects of eccentricity of the runway center, the system is simplified by the following assumptions.

1. No rolling resistance, i.e., $M_f = 0$.
2. At steady state, no drag force, i.e., $D = 0$.
3. At steady state, the rotor rotates at constant speeds, i.e., $\dot{\theta} = \omega$, and the balls are motionless relative to runway, i.e., $\dot{\phi} = \ddot{\phi} = 0$. The existence of the steady state motionless solution for the balls can be verified easily by numerical simulation.
4. The damping washers of the suspension system have the properties, $K_X = K_Y = K$ and $C_X = C_Y = C$.

For the sake of simplification, only a single ball with mass m is considered. With the assumptions made above, the system equation (7) at steady state can be simplified as

$$\begin{aligned} M\ddot{X} + C\dot{X} + KX &= M_R[\rho\omega^2\cos\omega t + e\omega^2\cos(\omega t+\beta)] \\ &\quad + m[\rho\omega^2\cos\omega t + R\omega^2\cos(\omega t+\phi_S)], \\ M\ddot{Y} + C\dot{Y} + KY &= M_R[\rho\omega^2\sin\omega t + e\omega^2\sin(\omega t+\beta)] \\ &\quad + m[\rho\omega^2\sin\omega t + R\omega^2\sin(\omega t+\phi_S)], \\ m[(\ddot{X} - \rho\omega^2\cos\omega t)\sin(\omega t+\phi_S) &- (\ddot{Y} - \rho\omega^2\sin\omega t)\cos(\omega t+\phi_S)] = 0, \end{aligned} \tag{8}$$

where ϕ_S is the steady state angular position of the ball. The first and second equations describe the C.G. motion of the stator and are in the form of linear second order equations with external harmonic excitations in identical frequencies. Due to the identity, the multiple harmonics on the R.H.S. of the first and second equations can be synthesized into two individual single harmonics, and then the solutions $X(t)$ and $Y(t)$ can be easily obtained. Substituting the solved $X(t)$ and $Y(t)$ into the third equation of equation (8), a time-independent algebraic equation can be acquired as follows to solve for ϕ_S which, defined in co-ordinate $O_rX_rY_r$, is the angular position of the ball relative to the rotating angle of the rotor θ at steady state.

$$C\omega[mR + eM_R\cos(\beta-\phi_S) + (m+M_R)\rho\cos\phi_S] - (K - M\omega^2)eM_R\sin(\beta-\phi_S) \tag{9}$$

$$+\left[\frac{(K-M\omega^2)^2 + (C\omega)^2}{\omega^2} + (K-M\omega^2)(m+M_R)\right]\rho\sin\phi_S = 0.$$

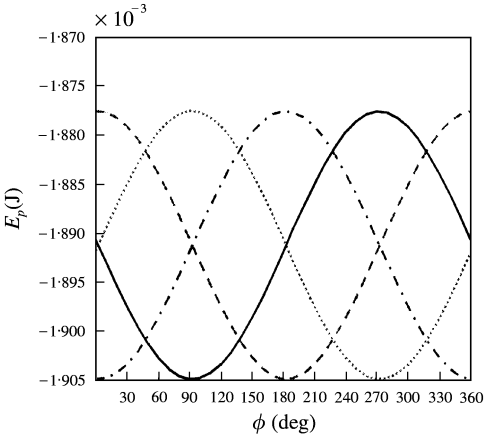

Figure 4. The relations between the potentials E_p and the angular position of the ball ϕ with runway eccentricity $\rho = 0$ and various β: – – – – –, $\beta = 0$; ·····, $\beta = \pi/2$; —·—, $\beta = \pi$; ——, $\beta = 3\pi/2$.

It can be calculated that there are two feasible solutions ϕ_S for equation (9). Through calculation of eigenvalues of equation (8) for each solution, the associated stability can be determined. Based on a number of computations, it is often bound that only one of the two feasible ϕ_S is stable. Due to the complexity of stability analysis involved, the process of computation is not elaborated herein.

With the stable solutions of ϕ_S, the steady state motion of the ball in view of inertial co-ordinates $O_R X_R Y_R$ can be easily obtained using the fact $\overline{O_R O_B} = \overline{O_R O_s} + \overline{O_s O_r} + \overline{O_r O_B}$, which can be presented in the following form:

$$\overline{O_R O_B} = A_B \cos(\omega t + \kappa)\vec{\mathrm{i}} + A_B \sin(\omega t + \kappa)\vec{\mathrm{j}}, \tag{10}$$

where

$$\begin{aligned} A_B = \frac{\omega^2}{A} \{ & (A + 2KM + m(m - 2M)\omega^2)(R^2 + \rho^2 + 2R\rho\cos\phi) \\ & + 2M_R(\rho + R\cos\phi)[(K + (m - M)\omega^2)(\rho + e\cos\beta) + Ce\,\omega\sin\beta] \\ & - 2M_R R\sin\phi(C\,\omega\rho + C\,\omega e\cos\beta) - e(K + (m - M)\omega^2)\sin\phi\sin\beta \\ & + M_R^2\omega^2(e^2 + \rho^2 + 2e\rho\cos\beta)\} \end{aligned}$$

and κ is the solved phase of ball oscillation observed from inertial co-ordinate $O_R X_R Y_R$, which is not shown herein due to its complexity. To avoid cumbersome stability analysis, a method based on simple physical rules by means of a potential-energy formulation for the ball is developed to make a quick judgment on which one of two ϕ_S solutions is stable. Define that the ball's potential is zero at $\phi = 0$, then at a given ϕ, the potential is

$$E_P = -\int_0^{\phi} m(A_B\omega^2)\,\mathrm{d}A_B = -\frac{1}{2}mA_B^2\omega^2. \tag{11}$$

Utilizing equation (11) and the expression of A_B in equation (10), the potentials versus ϕ with $\rho = 0$ and some values of β for the case of $M_R\, e = mR$ can be calculated and are shown in Figure 4. Note that the assumption $M_R\, e = mR$ refers to the case of perfect balance in which a single ball generates a counterbalance exactly equal to the inherent

unbalance of the rotor system. It can always be found in Figure 4 that the value of ϕ leading to the lowest potential corresponds to the stable solution of ϕ_S determined by stability analysis. Therefore, it is suggested that to simplify the computation process, one can calculate the potential formulated in equation (11) to determine which one of two feasible ϕ_s's is stable, and then the ball motion at steady state can be calculated by the harmonic form equation (10) with the determined stable ϕ_S.

The performance of the ball balancer is evaluated by the magnitude of the residual radial vibration of the rotor-balancer system, i.e., $A = \sqrt{X(t)^2 + Y(t)^2}$, which is derived by incorporating the solution equation of ϕ_S equation (9) into the first and second equations in equation (8) and solving for the periodic steady state solutions of $X(t)$ and $Y(t)$, which yields

$$X(t) = \frac{(K - M\omega^2)\omega^2}{(K - M\omega^2)^2 + (C\omega)^2}[(M_R + m)\rho\cos(\omega t) + M_R e\cos(\omega t + \beta) + mR\cos(\omega t + \phi_s)]$$

$$+\frac{C\omega^3}{(K - M\omega^2)^2 + (C\omega)^2}[(M_R + m)\rho\sin(\omega t) + M_R e\sin(\omega t + \beta) + mR\sin(\omega t + \phi_s)],$$

$$Y(t) = \frac{(K - M\omega^2)\omega^2}{(K - M\omega^2)^2 + (C\omega)^2}[(M_R + m)\rho\sin(\omega t) + M_R e\sin(\omega t + \beta) + mR\sin(\omega t + \phi_s)]$$

$$-\frac{C\omega^3}{(K - M\omega^2)^2 + (C\omega)^2}[(M_R + m)\rho\cos(\omega t) + M_R e\cos(\omega t + \beta) + mR\cos(\omega t + \phi_s)],$$

and then

$$A = \sqrt{X(t)^2 + Y(t)^2}$$

$$= \omega^2 \sqrt{\frac{(M_R + m)^2\rho^2 + (M_R e^2) + (mR)^2 + 2\rho e M_R(M_R + m)\cos\beta + 2me M_R R\cos(\beta - \phi_s) + 2\rho mR(M_R + m)\cos\phi_s}{(K - M\omega^2)^2 + (C\omega)^2}}. \tag{12}$$

For the case of $M_R e = mR$, Figure 5(a) shows the analytical solution A by equation (12) versus various ρ and β, while Figure 5(b) shows the corresponding solutions as directly obtained through simulating the dynamic model equation (7) by using SIMULINK, which indicate a good agreement with those obtained in Figure 5(a). From both Figures 5(a) and 5(b), it is seen that non-zero ρ gives rise to residual radial vibrations and this rise of vibrations is amplified around 90° of β. In other words, to reduce residual radial vibrations, one ought to control the eccentricity ρ to be as small as possible.

3.2. THE EFFECT OF ROLLING RESISTANCE

Several physical factors stated as follows are considered as the attributes of rolling resistance [13, 14].

1. Due to the fact that the balls and runway flanges are not perfectly rigid bodies, the deformations lead to a contact surface, instead of a point, between balls and runway flanges, which induces the rolling resistance.
2. The deformation process undergoes a cycle of elastic hysteresis that causes energy loss that also leads to an increase of rolling resistance.

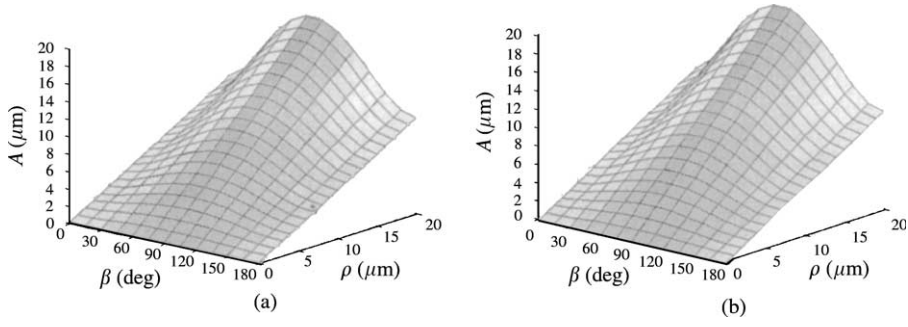

Figure 5. The residual radial vibration level A versus runway eccentricity ρ and the C.G. lead angle β for the case of perfect balance and $M_f = 0$. (a) Analytical results; (b) SIMULINK results.

3. The imperfections due to manufacture tolerance on the geometric shapes of runway surface and balls generate rolling resistance.

To understand the effects of rolling resistance on system dynamics, the assumptions utilized for the analysis in section 3.1 are also employed in this section. Incorporating the assumptions into equation (7), and assuming a single ball balancer with mass m for the sake of simplicity, the system equation (7) at steady state become

$$M\ddot{X} + C\dot{X} + KX = M_R[\rho\omega^2\cos(\omega t) + e\omega^2\cos(\omega t + \beta)] + m[\rho\omega^2\cos(\omega t) + R\omega^2\cos(\omega t + \phi_S)], \tag{13a}$$

$$M\ddot{Y} + C\dot{Y} + KY = M_R[\rho\omega^2\sin(\omega t) + e\omega^2\sin(\omega t + \beta)] + m[\rho\omega^2\sin(\omega t) + R\omega^2\sin(\omega t + \phi_S)], \tag{13b}$$

$$|m\{[\ddot{X} - \rho\omega^2\cos(\omega t)]\sin(\phi_S - \omega t) - [\ddot{Y} - \rho\omega^2\sin(\omega t)]\cos(\phi_S + \omega t))| \leqslant \left|\frac{M_f}{r}\right|, \tag{13c}$$

where equation (13c) indicates that at steady state the inertial forces generated by balls must be smaller than or equal to the resistant force generated by rolling resistance M_f.

Conducting the same process as used previously, ϕ_S, the steady state angular position of the ball, can be calculated using equation (13) as follows, which is derived by solving equations (13a), (13b) for $X(t)$ and $Y(t)$, and substituting them into equation (13c).

$$\left|\frac{m\omega^2[mRC\omega + eC\omega Mr\cos(\beta - \phi_S) - eMr(k - M\omega^2)\sin(\beta - \phi_S)]}{(K - M\omega^2)^2 + (C\omega)^2}\right| \leqslant \left|\frac{M_f}{r}\right|. \tag{14}$$

In what follows, $(\beta - \phi_S)$ replaces ϕ_S to characterize the steady state ball position due to the particular complexity involved in equation (14). Based on equation (14), a complete balance, i.e., $X(t) = Y(t) = 0$, is not necessarily achieved due to the existence of a non-zero, small M_f, even when $\rho = 0$ and $M_R e = mR$. For an easy computation of unbalance level, $(\beta - \phi_S)$ is chosen to serve as a valid indicator for characterizing levels of unbalance due to the following two facts. First, as $\rho = 0$, to achieve a complete balance, $(\beta - \phi_S)$ must be equal to 180°rendering R.H.S. of equations (13a, b) equal to zero. Secondly, a deviation of $(\beta - \phi_S)$ from 180° increases levels of residual radial vibrations.

Inequality (14) is next solved for $(\beta - \phi_S)$ to obtain the steady state angular position of the ball. Based on the inequality form of equation (14), for a given value of rolling resistance

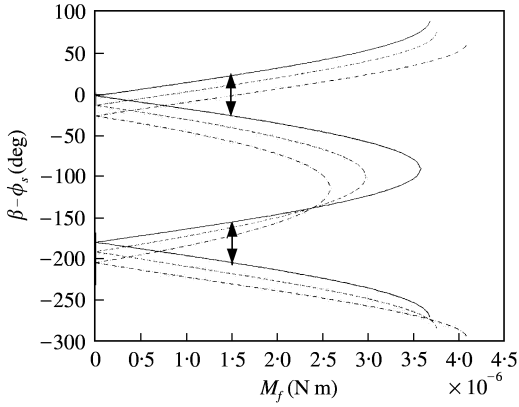

Figure 6. The solutions of $(\beta - \phi_S)$ versus various values of rolling resistance M_f with runway eccentricity $\rho = 0, 1, 2$ μm: ——, $\rho = 0$ μm; – – – –, $\rho = 1$ μm; —·—, $\rho = 2$ μm.

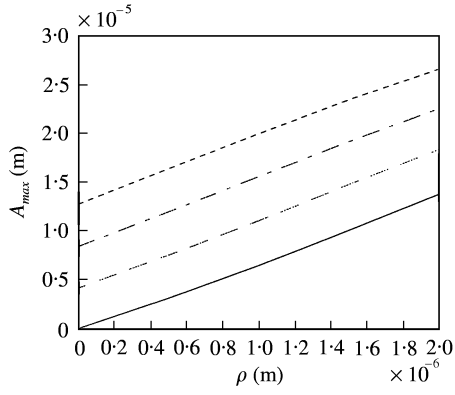

Figure 7. The maximum residual radial vibration levels A_{max} versus various values of runway eccentricity ρ with $M_f = 0, 0{\cdot}5 \times 10^{-6}$, 1×10^{-6}, $1{\cdot}5 \times 10^{-6}$, $\beta = 60^\circ$; ——, $M_f = 0$ N m; – – – –, $M_f = 0{\cdot}5 \times 10^{-6}$ N m; – – –, $M_f = 1{\cdot}0 \times 10^{-6}$ N m; ·····, $M_f = 1{\cdot}5 \times 10^{-6}$ N m.

M_f, there exist multiple distinct solutions for $(\beta - \phi_S)$ which form continuous finite ranges. The distinct solutions of $(\beta - \phi_S)$ in these finite ranges will lead to distinct residual unbalance levels A's, yielding an inconsistency in balancing effectiveness. Figure 6 shows the solved $(\beta - \phi_S)$ values versus various M_f for the case of perfect balance; i.e., $M_R e = mR$, and three different values of ρ, where for each value of ρ two finite ranges between the curves and prescribed by arrows in the figure indicate two sets of the feasible solutions of $(\beta - \phi_S)$. It is seen from Figure 6 that as rolling resistance M_f increases, the range of $(\beta - \phi_S)$ is enlarged and even equal to 360° as M_f approaches $M_f = 3{\cdot}7 \times 10^{-6}$, resulting in a serious problem of inconsistency. Therefore, one needs to ensure a small M_f to minimize feasible ranges of $(\beta - \phi_S)$ solution for a satisfactory consistency. It is also seen from Figure 6 that as ρ varies, for a given M_f, a slight increase in runway eccentricity ρ induces a phase-shift-like effect on $(\beta - \phi_S)$ but leaves the sizes of solution ranges of $(\beta - \phi_S)$ almost unchanged. Therefore, the effect of ρ on the consistency is insignificant.

With the solutions of $(\beta - \phi_S)$ in hand, the corresponding residual radial vibration levels A's are next computed for $\beta = 60^\circ$, various ρ, M_f and $M_R e = mR$. The results are shown in

Figure 7 where A_{max} is used to capture the maximum values of A for all possible solutions of $(\beta - \phi_S)$ with given values of β, M_f and ρ. It can be seen that A_{max} increases as runway eccentricity ρ and rolling resistance M_f increase.

3.3. THE EFFECT OF DRAG FORCE

The drag force induced by the dynamic interaction between the ball and the fluid-filled runway is formulated and analyzed herein to investigate its effects on system transient response. The drag force is assumed to be in the following form [15]:

$$D = -\tfrac{1}{2} C_D \rho_{flow} V_{rel}^2 \bar{A} \operatorname{sign}(V_{rel}), \tag{15}$$

where V_{rel} is the relative speed of ball to the fluid, C_D is the drag coefficient that is a function of ball size, shape, surface roughness and dynamic viscosity, ρ_{flow} is fluid density and $\bar{A}$ is the frontal area of ball. From equation (15), one can see that D vanishes as the ball reaches its steady state, i.e., $V_{rel} = 0$.

To understand the effects of various types of fluids on transient responses, the following assumptions are made for simplification.

1. The balls have smooth surfaces.
2. The fluid is uniformly distributed in runway and motionless relative to runway.

Based on the above assumptions and force balance of the balls, the equations of motion for the system with a single ball equivalently can be rewritten as

$$\begin{aligned}
M\ddot{X} + C\ddot{X} + KX &= M_R[e\ddot{\theta}\sin(\theta+\beta) + e\dot{\theta}^2\cos(\theta+\beta)] \\
&\quad + m[R(\ddot{\theta}+\ddot{\phi})\sin(\theta+\phi) + R(\dot{\theta}+\dot{\phi})^2\cos(\theta+\phi)] \\
M\ddot{Y} + C\ddot{Y} + KY &= M_R[-e\ddot{\theta}\cos(\theta+\beta) + e\dot{\theta}^2\sin(\theta+\beta)] \\
&\quad + m[-R(\ddot{\theta}+\ddot{\phi})\cos(\theta+\phi) + R(\dot{\theta}+\dot{\phi})^2\sin(\theta+\phi)] \\
\left(m + \frac{1}{r^2}\right) R(\ddot{\phi}+\ddot{\theta}) &= m[\ddot{X}\sin(\phi+\theta) - \ddot{Y}\cos(\phi+\theta)] \\
&\quad - \frac{1}{2} C_D \rho_{flow} (R\dot{\phi})^2 (\pi r^2) \operatorname{sign}(\dot{\phi}) + \frac{(R+r)}{r^2} I\ddot{\theta}.
\end{aligned} \tag{16}$$

The software SIMULINK is next used to simulate the system response with rotating speed increased from 0 to 2·5 orders (2·5 times of suspension natural frequency) in 2 s. When the fluid filling the runway is air, the ball takes more than 10 s to reach steady state. If the fluid is SAE 30 oil, the ball balancer is able to reach steady state in less than 10 s. Although both experimental results are far from satisfying the industrial standard on response time requirement, these do indicate that drag force has a damping-like effect on the system transient response, which reveals the potential to help stabilize the desired steady state solution and to decrease response time.

Designers of rotor–balancer systems can refer to analytical results obtained in sections 3.1–3.3 to find the optimum design parametric values possible for runway eccentricity and rolling resistance, and choose the right fluid under the limitations imposed by system nature. General design guidelines for tuning these three parameters are decreasing runway and C.G. eccentricity, minimizing rolling resistance and choosing such a fluid to fill runway that leads to a smooth and fast transient response.

Figure 8. Photograph of the experimental apparatus.

4. EXPERIMENTAL STUDY

Experimental study is next performed to verify the validity of the established mathematical model in order to ensure the legitimacy of the analytical results obtained and design guidelines proposed.

4.1. DESIGN OF EXPERIMENTAL APPARATUS

Figure 8 shows a photograph of the experimental apparatus which includes seven subsystems: a balancer system composed of a circular runway and a ball inside, a test disk, a spindle motor accompanied with a driving circuit, the motor supporting structure, an accelerometer unit, a stroboscope and a signal analyzer.

The circular runway of the balancer system was made of aluminum alloy with an inner radius of 16·5 mm. A thin, cylindrical glass ring was press-fitted inside the runway in order to make the contact surface between the ball and runway smooth enough so that the rolling resistance was greatly reduced. The runway eccentricity was obtained by placing a precision dial gauge perpendicular to runway wall and measuring the rotating radii as circular runways rotate 360°. A test disk was attached firmly on the motor–balancer assembly through a magnetic holding device in an annular shape. The inherent unbalance of the rotor system was identified prior to experiments, simply by placing a point mass on the circumference of the disk three times at distinct positions with 120° span and summing up the corresponding unbalance in the form of vectors, which is 0·272 g cm. The ball weighs 0·261 g, leading to an unbalance of 0·43 g cm which is larger than the unbalance of the rotor system. A set comprising a spindle motor and its driver widely used commercially for a variety of optic disk drives is chosen for experiments. The motor base structure assimilated to washer flexibility was built using four L-shaped beams stretched horizontally

TABLE 1

Applied system parameter values

System parameters	Applied values	Reference values from commercial optic drives
Natural frequency ω_n (f_0)	21·2 Hz	40–50 Hz
Mass of equivalent stator M_S	102 g	$M = M_S + M_R + nm$
Mass of equivalent rotor M_R	36·1 g	Total mass M: 100–150 g
Ball mass m	0·261 g	Disk mass M_{disk}: around 15·8 g
Ball radius r	1·25–2 mm	1·25 mm
Runway radius R	16·5 mm	15 mm
Suspension stiffness K_X, K_Y	2455 N/m	$K = M\omega_n^2$
Suspension damping ratio ζ	0·025	0·1 for rubber 0·05 for plastic 0·025 for metal
C.G. eccentricity e	0·068 mm	around 0·5 mm
Runway eccentricity ρ	0·01 mm	0·001–0·05 mm

to positive and negative X, Y directions. These four beams were designed to have cross-sections with much larger vertical thickness than horizontal in order to induce a much larger vertical rigidity for the beams. This large rigidity in fact restricts the vertical motion of the balancer–motor assembly greatly. The accelerometers are attached horizontally on the supporting structure to record the accelerations in X, Y directions. The dimensions of the four beams were designed to specify horizontal natural frequencies for the structure, $\omega_{nX} \approx \omega_{nY} \approx 21{\cdot}2$ Hz that was controlled to be well below the operating speeds of disk drives. Table 1 lists related parameter values of the experimental apparatus.

4.2. EXPERIMENTAL PROCESS

A schematic of the instrumentation used in the experimental process is presented in Figure 9. In the process, the motor was first powered by a power supply unit through the driver to accelerate the rotation of rotor up to desired speeds. In the meantime, the driver also sent a speed signal to the stroboscope for tuning its flashing frequency in synchrony with the rotating speeds in order to observe the steady state angular position of the ball balancer. As the ball settled to its steady state, the ball angular position was recorded manually, while the accelerations of the motor–balancer unit in X, Y directions were measured by accelerometers, recorded by the analyzer, and converted to radial displacements by a simple MATLAB program.

4.3. EXPERIMENTAL RESULTS

With ρ calibrated around 0·4 μm, Figure 10 shows both experimental and analytical results for the phase difference between the angular positions of the disk C.G. and ball, $(\beta - \phi_S)$, with respect to various speed ratios. It can be seen that most of the experimental data of $(\beta - \phi_S)$ are located in the range within theoretical upper/lower bounds corresponding to a non-zero rolling resistance $M_f = 1{\cdot}5 \times 10^{-6}$, except for those near natural frequency (speed ratio $\leqslant 2$). This is due to the fact that in the neighborhood of

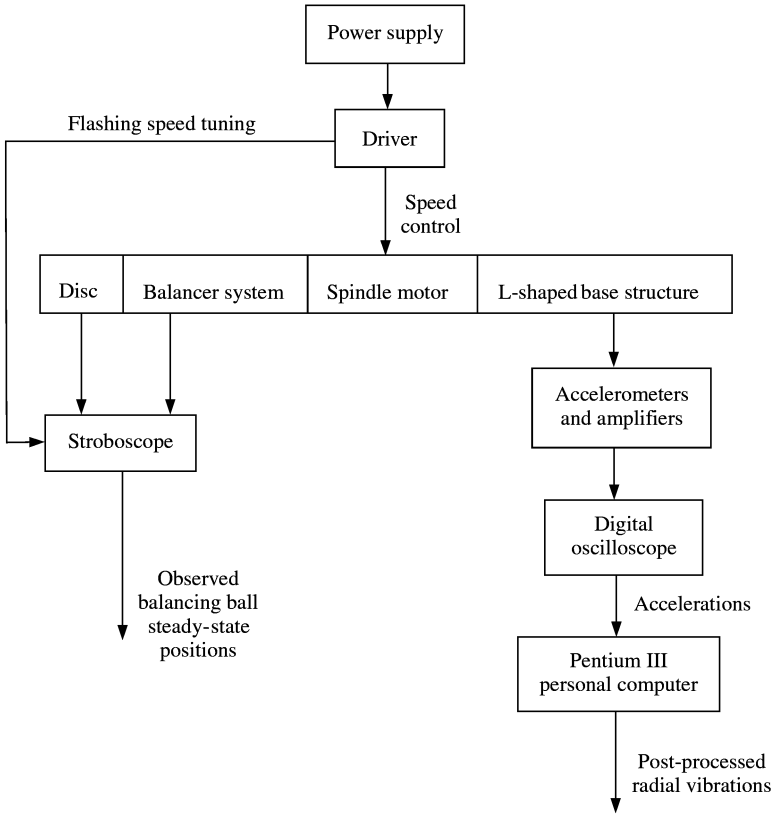

Figure 9. Schematic of experimental instrumentation.

natural frequency resonance significantly enlarges the levels of vibration which causes rolling friction to dominate the system dynamics and then leads to unpredictable steady state of ball position. It is also shown in Figure 11 that experimental residual radial vibration levels are close to the theoretical predictions as speed varies. The results shown in Figures 10 and 11 verify the capability of the mathematical model constructed in the previous section.

5. CONCLUSION

This study investigated the dynamics effects of runway eccentricity, rolling resistance and drag force on a rotor–balancer system that is designed to reduce residual unbalanced vibrations. The results were obtained by formulating the equations of motion, solving for steady state solutions, and verifying them by numerical simulations. It was found that non-zero runway eccentricity and rolling resistance contributed to an increase in residual vibrations, while the existence of drag force improved transient response. With the analysis completed, design guidelines were readily provided for designers for controlling the aforementioned system parameters to their optimal values in order to reduce residual vibrations to minima. Experiments were also designed and conducted to verify theoretical results. A satisfactory agreement was confirmed between theoretical and experimental results.

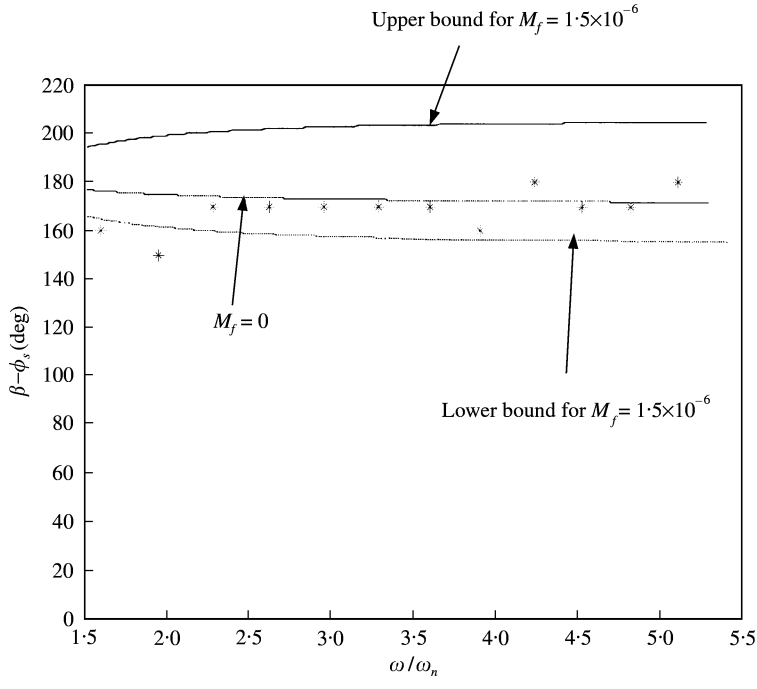

Figure 10. Theoretical and experimental phase differences between the C.G. and the ball ($\beta - \phi_S$) versus speed ratios ω/ω_n: *, experimental measurements; —, theoretical predictions.

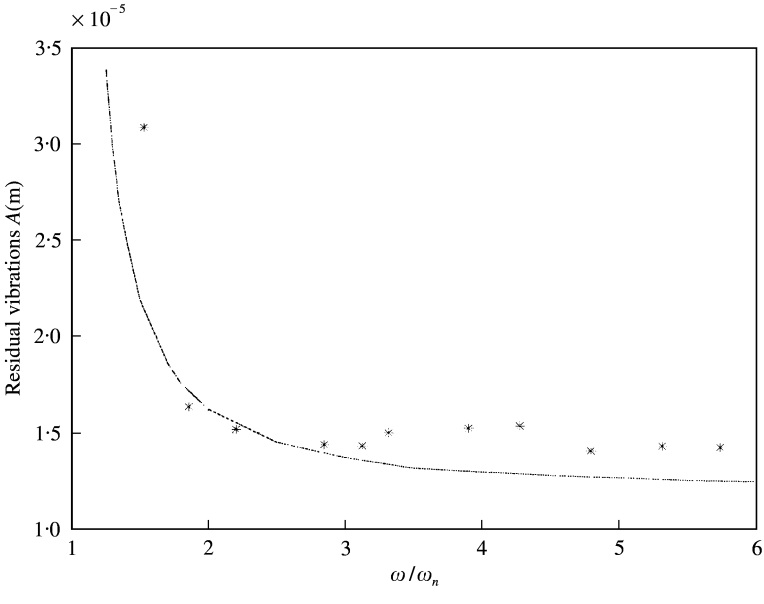

Figure 11. Theoretical and experimental residual vibration levels A versus speed ratios ω/ω_n: *, experimental measurements; —, theoretical predictions.

ACKNOWLEDGMENTS

The authors would like to express special thanks to National Science Council of Republic of China for financially supporting this research project. The Contract No. is NSC88-2212-E-007-030.

REFERENCES

1. E. L. THEARLE 1950 *Machine Design* **22**, 119–124. Automatic dynamic balancers (Part 1—Leblanc balancer).
2. E. L. THEARLE 1950 *Machine Design* **22**, 103–106. Automatic dynamic balancers (Part 2—Ring, pendulum, ball balancers).
3. J. INOUE, Y. JINNOUCHI and S. KUBO 1979 *Transactions of the Japan Society of Mechanical Engineers, Part C* **49**, 2142–2214. Automatic balancers.
4. P. BÖVIK and C. HÖGFORS 1986 *Journal of Sound and Vibration* **111**, 429–444. Autobalancing of rotors.
5. Y. JINNOUCHI, Y. ARAKI, J. INOUE, Y. OHTSUKA and C. TAN 1993 *Transactions of the Japan Society of Mechanical Engineers, Part C* **59**, 79–84. Automatic balancer (static balancing and transient response of a multi-ball balancer).
6. T. MAJEWSKI 1988 *Mechanism and Machine Theory* **23**, 71–77. Position errors occurrence in self balancers used on rigid rotors of rotating machinery.
7. C. RAJALINGHAM and S. RAKHEJA 1998 *Journal of Sound and Vibration* **217**, 453–466. Whirl suppression in hand-held power tool rotors using guided rolling balancers.
8. J. CHUNG and D. S. RO 1999 *Journal of Sound and Vibration* **228**, 1035–1056. Dynami analysis of an automatic dynamic balancer for rotating mechanism.
9. K. TAKASHI, S. YOSHIHIRO, Y. YOSHIAKI, S. SHOZO and M. SHIGEKI 1998 *Japanese Patent* 10,092,094. Disk type storage device.
10. M. KIYOSHI, M. KAZUHIRO, Y. SHUICHI, F. MICHIO, U. TOKUAKI and K. MASAAKI 1997 *Japanese Patent* 10,083,622. Disk drive device.
11. Y. TAKATOSHI 1998 *Japanese Patent* 10,188,46. Disk drive device.
12. K. MASAAKI 1998 *Japanese Patent* 10,208,37. Disk device.
13. E. RABINOWICZ 1965 *Friction and Wear of Materials*. New York: John Wiley & Sons, Inc.
14. R. DRUTOWSKI 1959 *Friction and Wear*. New York: Elsevier Publishing Company. Energy losses of ball rolling on plates.
15. B. R. MUNSON, D. F. YOUNG and T. H. OKIISHI 1990 *Fundamentals of Fluid Mechanics*. New York: John Wiley and Sons, Inc.